A Novel Quasi-Emulsion Solvent Diffusion-based Spherical Cocrystallization Strategy for Simultaneously Improving the Manufacturability and Dissolution of Indomethacin

Hongbo Chen[a], Hongyun Xu[b], Chenguang Wang[a], Hyunho Kang[c], Christy L. Haynes[c], Mahesh K. Mahanthappa[b], and Changquan Calvin Sun[a,*]

[a] Pharmaceutical Materials Science and Engineering Laboratory, Department of Pharmaceutics, College of Pharmacy, University of Minnesota, Minneapolis, MN 55455, USA

[b] Department of Chemical Engineering and Materials Science, University of Minnesota, Minneapolis, MN 55455, USA

[c] Department of Chemistry, University of Minnesota, Minneapolis, MN 55455, USA

**Corresponding author*

Changquan Calvin Sun, Ph.D.

9-127B Weaver-Densford Hall

308 Harvard Street S.E.

Minneapolis, MN 55455

Email: sunx0053@umn.edu

Tel: 612-624-3722

Fax: 612-626-2125

Abstract

Successful development of tablet formulations of many active pharmaceutical ingredients (APIs) is challenged by their poor manufacturability (e.g., flowability, tabletability) and dissolution characteristics. Here, we report a novel quasi-emulsion solvent diffusion cocrystallization (QESD-CC) method as an integrated crystal and particle engineering approach for successful generation of spherical cocrystal agglomerates of the poorly soluble drug indomethacin (IMC) and the sweet co-crystallization agent saccharin (SAC). The QESD-CC process consists of two distinct steps: 1) formation of a transient emulsion containing solvated IMC and SAC, and 2) subsequent precipitation of IMC-SAC cocrystals from the emulsion as hollow spherical particles. Solution ^{1}H NMR analyses and computational modeling studies indicated that hydroxypropyl methylcellulose (HPMC) preferentially interacts with the SAC molecules through hydrogen bonds, thus driving the polymer to form a shell that stabilizes the transient emulsion droplets and coats the resulting particles. Spherical QESD-CC particles exhibited excellent flowability, while the HPMC coating and micro-size primary crystals led to excellent tabletability. Outstanding manufacturability and high cocrystal solubility thus enabled the successful development of a high drug loading tablet formulation comprising 46.3 wt% IMC.

Introduction

Tablet manufacturing by direct compression (DC) processes is attractive to the pharmaceutical industry because of its cost effectiveness. DC tableting is particularly suitable for continuous manufacturing due to its procedural simplicity.[1] For typical active pharmaceutical ingredients (APIs) with doses ≥ 100 mg, high API-loaded tablet formulations are preferred to reduce tablet size, making them easier to swallow and thus enhancing patient compliance. However, a DC tablet formulation typically does not contain more than 30 wt% API due to its common and undesirable physical properties, including poor powder flowability, poor tabletability, and poor water solubility, which requires the use of large amounts of solubilizing excipients to enable adequate therapeutic absorption.[2-4] APIs exhibiting both poor powder properties and low solubility consequently present a major challenge for developing a DC tablet formulation.

Spherical crystallization is an established technique for improving micromeritic properties (e.g., particle size, shape, bulk density) of drugs by agglomerating the small primary crystals into large and spherical agglomerates, mainly by spherical agglomeration (SA)[5-7] and quasi-emulsion solvent diffusion (QESD) techniques.[8, 9] In fact, spherical crystallization of water-soluble ferulic acid enabled the development of a DC tablet formulation containing a record high 99% API.[3] However, spherical crystallization often detrimentally impacts the rate of drug release of poorly soluble APIs because this process reduces the exposed surface area available for dissolution.[10]

The problem of slow dissolution of poorly soluble APIs may be addressed by the use of solubilizing excipient(s) in tablet formulations. However, this approach invariably leads to large tablets due to the significant amounts of solubilizing excipient required. Another effective

approach is to use a soluble solid form of the poorly soluble API, such as an amorphous solid dispersion (ASD),[11] a salt,[12] or a cocrystal.[13] Among these options, ASD requires the use of a large amount of excipient as a matrix to maintain adequate physical stability against crystallization[14] as well as a high dissolution rate of the API.[15, 16] Salt formation is applicable only to ionizable APIs and is limited by the availability of pharmaceutically acceptable counterions.[17] In comparison to ASD and salt formation, cocrystals exhibit unique advantages for enhancing dissolution of poorly soluble APIs because they are physically stable in solid state, applicable to non-ionizable molecules, and the number of pharmaceutically acceptable co-formers is substantial.[17, 18] However, use of these more soluble solid forms confers manufacturability challenges for high dose DC tablet formulations, since the tablet weight fraction of these solid forms required for the same dose of API is invariably higher than that of the parent API. To ensure acceptable manufacturability, micromeritic properties of the new API solid form cannot be poor in order to maintain a high API loading in the tablet.

Spherical cocrystallization (SCC) has the potential to simultaneously improve both tablet manufacturability and API dissolution performance.[19, 20] Although earlier work successfully demonstrated that SCC of griseofulvin (GSF) with the co-former Acesulfame (Acs) profoundly improves flowability and dissolution characteristics, the tableting performance of spherical GSF-Acs cocrystal agglomerates remained poor, which limited the ultimate GSF loadings per tablet.[19] The reason for the poor tabletability of GSF-Acs was the large average size of the primary crystals in the spherical agglomerates, which led to small interparticle bonding areas and consequently weak tablets.[21] The large size of primary cocrystals was attributed to the use of a slurry cocrystallization process, which allowed formation of large cocrystals. Hence, an improved SCC process that produces spherical cocrystal agglomerates consisting of finer

primary crystals has the potential to enable the development of high dose DC tablets by simultaneously improving the flowability, tabletability, and dissolution of APIs. To attain this goal, we developed a novel quasi-emulsion solvent diffusion cocrystallization (QESD-CC) process. In contrast to slurry cocrystallization, QESD-CC exhibits the potential to yield large and spherical particles consisting of much smaller primary cocrystals due to the high degree of supersaturation during QESD,[22] leading to better tabletability and flowability while retaining a high dissolution rate. A successful QESD-CC process requires that the following two conditions are met: 1) formation of sufficiently stable transient emulsions of co-formers, and 2) reaction between API and co-former to form a cocrystal upon solvent counter-diffusion. In this work, we chose indomethacin (IMC)-saccharin (SAC) cocrystal as a model system,[23] and HPMC as an emulsion stabilizer because of its successful use in QESD processes.[24-26] Since the IMC-SAC cocrystal exhibits much higher solubility than neat IMC (13 times greater in water and 13-65 times higher at pH 1-3),[27] it can likely improve the dissolution of IMC.

Materials and methods

Materials

Indomethacin (γ-IMC, Tokyo Chemical Industry, Tokyo, JP) and saccharin (SAC, Carbosynth Limited, Berkshire, UK), were chosen as the model API and co-former, respectively. Microcrystalline cellulose (Avicel PH102, FMC, Philadelphia, PA), HPMC (K100M, MW 1,000 kg/mol, Ashland Specialty Ingredients, Wilmington, DE), croscarmellose sodium (CCM-Na, SD-711, FMC Biopolymer, Philadelphia, PA), magnesium stearate (MgSt, Mallinckrodt Inc., St. Louis, MO), dimethylformamide (Fisher Scientific, Hampton, NH), methanol (Fisher Scientific, Hampton, NH) and ultrapure deionized water (0.066 μS/cm, Thermo Scientific, USA) were used

as received. The chemical structures of IMC, SAC, and HPMC are shown in Figure 1. All crystallization experiments were performed in glass beakers.

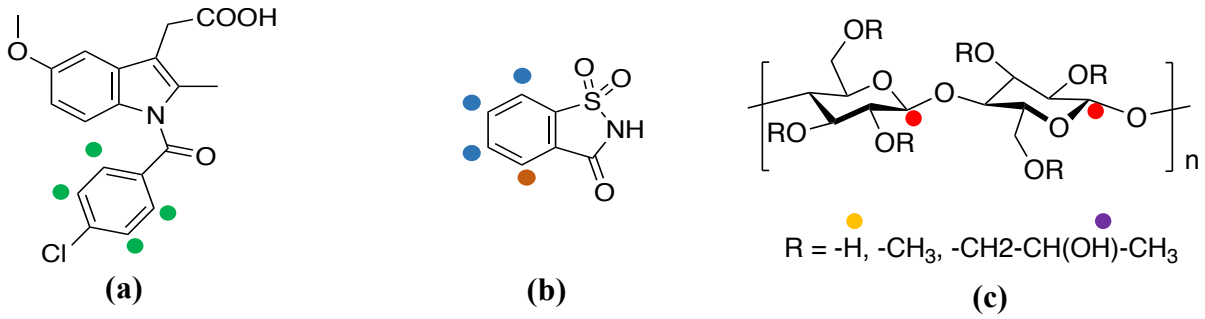

Figure 1. Chemical structures of (a) IMC, (b) SAC and (c) HPMC. Hydrogen atoms that participate in intermolecular interactions responsible for QESD-CC are marked with different colors in accordance to their chemical shifts in solution ^{1}H NMR spectra.

Preparation of IMC-SAC cocrystal powders

Fine IMC-SAC cocrystals by anti-solvent method: Based on a literature study,[23] a substantial excess of SAC was required to account for the large solubility difference between IMC and SAC to ensure phase purity of the produced cocrystal powder. Therefore, 5 mmol of IMC and 15 mmol of SAC were co-dissolved in 140 mL of MeOH. The MeOH solution was then rapidly poured into 140 mL of H2O in ≤ 10 s and mixed with a magnetic stirring bar under ambient conditions for 30 min to produce fine IMC-SAC cocrystals. The resulting suspension was filtered and dried at 60 °C overnight to obtain a powder, hereafter referred as AS. The yield for this process was 70%. A small amount of this powder was dispersed onto a glass slide for analysis under a polarized light microscope (Eclipse E200; Nikon, Tokyo, Japan).

IMC-SAC spherical cocrystal agglomerates by QESD-CC method: A solution of 4 mmol IMC and 5 mmol SAC in 6 mL DMF was poured (in ≤10 s) into 40 mL of distilled H_2O or

0.01%, 0.1%, and 0.5% (*w*/*v*) HPMC aqueous solutions. A HPMC solution at ≥1% concentration was not attempted, due to its substantial viscosity that prevents effective mixing. Our preliminary work also suggested that DMF:H_2O ratios significantly deviating from 6:40 tended to cause phase impurity in the cocrystal. Phase purity in the cocrystal powders could only be achieved by increasing the relative amount of SAC. The suspension was agitated at 300 rpm using an overhead stirrer for 3 h at 23.5 ^oC to ensure complete transformation into IMC-SAC. This agitation speed was selected because it generated spherical agglomerates with a desirable particle size distribution (200-500 μm). The produced solid particles were filtered and dried, without solvent washing steps, at 60 °C overnight to yield a powder, hereafter referred as QESD-CC. A small amount of this powder was dispersed on a glass slide for imaging by polarized light microscopy.

Particle size distribution (PSD)

The particle sizes of as-received IMC, AS, and QESD-CC powders were determined using a particle size analyzer (Microtrac SIA, Montgomeryville, PA). Approximately 25 mg of each powder was suspended in Isopar G Fluid (~5 mL). The as-received IMC and AS samples were sonicated for 30 s to fully disperse the particles. The IMC-SAC and HPMC constituents of the QESD-CC powder exhibit negligible solubility in this medium. The suspension was added into a sample delivery controller (SDC, Montgomeryville, PA) and circulated through the closed system. A high-speed camera captured images of particles in focus. Using the Microtrac Flex image analysis software provided with the instrument, the diameter of a circle with an area equivalent to the projected area of individual particles was determined. The volume of the particle was calculated assuming a spherical shape to determine the volume distribution of a powder.

Specific surface area (SSA) measurement

Nitrogen adsorption-desorption isotherms for each sample were obtained using a surface area analyzer (Micromeritics ASAP 2020, Norcross, GA) at 77 K. Before each measurement, 0.5–1.0 g of accurately weighed sample was placed into a glass tube and degassed under high vacuum (15 μm Hg) at 27 °C for at least 24 hrs. The amount of the adsorbed nitrogen at different partial pressures of nitrogen in helium carrier gas was measured at a temperature of 77.35 K (Table S1). The Brunauer–Emmett–Teller (BET) equation[28] was used to fit the data and to calculate the sample surface area. All measurements were made in triplicate.

HPMC content determination via size-exclusion chromatography (SEC)

HPMC concentrations were determined by size exclusion chromatography (SEC) with refractive index detection.[29] SEC measurements were carried out on an Agilent 1260 liquid chromatograph equipped with one guard column and three separating CATSEC columns with pore sizes of 1000, 300 and 100 Å, operating in 0.1 M $Na_2SO_4(aq)$ containing 1 wt% acetic acid using an eluent flow rate of 0.4 mL/min at 22 °C. Analyte detection relied on a Wyatt Optilab T-rEX refractive index (RI) detector and a Wyatt Dawn Heleos II multi-angle static light scattering detector. The peak area from RI detector signal that corresponds to HPMC elution was used to determine the HPMC concentration in the *ASTRA* software. Using a pure HPMC (K100M) solution with 0.81 mg/mL concentration, the refractive index increment (*dn/dc*) of HPMC was determined to be 0.1165 mL/g (assuming 100% mass recovery on elution). The accuracy of this analytical method was then validated by quantifying the concentrations of five HPMC solutions prepared with concentrations ranging 0.45–1.04 mg/mL, for which the values obtained by SEC analyses agreed within 99.6% (see Figure S7 for details). Using this method, the amount of HMPC in the QESD-CC powders was subsequently quantified by dissolving ~0.65 g QESD-CC

in 5 mL THF (HPLC grade) to precipitate the HPMC. THF was selected as the precipitation solvent for HPMC, based on our observation that the solubility of HPMC in THF is ⩽ 0.75 mg HMPC/100 mL THF from gravimetric analyses. The precipitate was isolated by centrifugation (11 644 *g*, 10 min), after which the supernatant THF solution containing IMC and SAC was carefully decanted. The isolated HPMC was re-dispersed in 5 mL THF to wash away residual IMC and SAC by sonication for 10 min, and it was again isolated by centrifugation. The polymer was then dried under vacuum to remove residual THF. The isolated HPMC from the QESD-CC samples was dissolved in 5 mL SEC eluent and the concentration determined from the aforementioned calibration curve. The reported HPMC content in QESD-CC was determined as the average of three independent measurements.

Powder X-ray Diffractometry (PXRD)

The crystallographic properties of samples were characterized by powder X-ray diffractometer with Cu K_α radiation (1.54059 Å). Samples were scanned over the range $5 \leq 2\theta \leq 35°$ with a step size of 0.02° and a dwell time of 1 s/step. The divergence and anti-scattering slits on the incident beam path were 1/16 and 1/8 degree, respectively, and the antiscattering slit on the diffracted beam path was 5.5 mm (X'Celerator). The X-ray tube voltage and amperage were 45 kV and 40 mA, respectively. A theoretical PXRD pattern of IMC-SAC was calculated from the single crystal structure (CCDC refcode: UFERED).[30]

Thermal Analyses

Powder samples (~ 5 mg) were loaded into hermetic aluminum pans and heated from 30 to 190 °C at a heating rate of 10 °C/min on a differential scanning calorimeter (Q1000, TA Instruments, New Castle, DE) under a continuous helium purge at a flow rate of 25 mL/min.

DSC heat flow was calibrated with the enthalpy of melting of indium, and the temperature was calibrated with the melting transitions of indium and cyclohexane. To determine the volatile content, each sample (~ 5 mg) was placed in an open aluminum pan and analyzed on a thermogravimetry analyzer (Q500, TA Instruments, New Castle, DE). All samples were heated from room temperature to 300 °C at 10 °C/min under 25 mL/ min nitrogen purge.

Scanning electron microscopy (SEM)

Samples were mounted onto stubs with carbon tape. A thin platinum layer (thickness ~ 75 Å) was coated onto the samples using an ion-beam sputter coater (IBS/TM200S; VCR Group Inc., San Clemente, CA). The particle morphology and surface features were evaluated by scanning electron microscopy (JEOL 6500F; JEOL Ltd., Tokyo, Japan), operated in SEI mode with an accelerating voltage of 5 kV under high vacuum (10^{-4}-10^{-5} Pa).

Computational methods

Energy framework and topological analyses of crystal structures

Pairwise intermolecular interaction energies (Table S2) were estimated using CrystalExplorer and Gaussian09 from the experimental geometries of the IMC-SAC cocrystal and IMC (γ form, CSD refcode: INDMET).[31, 32] The hydrogen positions were normalized to standard neutron diffraction values prior to calculation using the CE-B3LYP electron densities model. The total intermolecular interaction energy for a given molecule is the sum of the electrostatic, polarization, dispersion, and exchange-repulsion components with scale factors of 1.057, 0.740, 0.871, and 0.618, respectively.[33] Intermolecular interaction between two molecules is ignored when the closest interatomic distance was > 3.8 Å. Interaction energies were visualized as a framework by connecting centers of mass of molecules with cylinder thicknesses

proportional to the total intermolecular interaction energies, where interaction energies weaker than -10 kJ/mol were omitted for clarity. The crystal packing topology was analyzed using a Python program.[34]

Drug–Polymer Intermolecular Interaction

To characterize the molecular interactions between IMC-SAC and HPMC, optimization of their complexation was performed in Gaussian16 using DFT hybrid functional M06 level of theory and 6-31(d, p) basis sets.[35, 36] To reduce the computational cost, three different monomer units bearing different substituents (R = H, CH_3, or $CH_2CH(OH)CH_3$ in Figure 1) of HPMC were used. The IMC-SAC complex was from the reported structure (UFERED). Structure optimization was carried out without any constraints and local minima energies were confirmed through vibrational frequency calculations. The final optimized complexes were used to identify the possible intermolecular hydrogen bond formation.

Preparation of formulated powders

Different powder forms of IMC and all other excipients (Table 1), totaling approximately 5 g, were added to a 30 mL plastic bottle, which was manually rotated about the long axis at an angle of 45^o to the horizon for 15 min (approximately 900 turns). A tablet formulation containing 46.3 wt% IMC in the same matrix was also prepared as a control. Avicel PH102 was used as the dry binder in all three formulations due to its high plasticity, acceptable flowability, and excellent tabletability.[37, 38] CCM-Na and MgSt functioned as a tablet super-disintegrant and a lubricant, respectively.

Table 1. Formulation composition of IMC-containing tablets using different IMC forms

Material	Function	IMC	AS	QESD-CC
IMC/IMC-SAC	API	46.3 %	70 %	70 %
Avicel PH102	Binder	48.2 %	24.5 %	24.5 %
CCM-Na	Super-disintegrant	5.0 %	5.0 %	5.0 %
MgSt	Lubricant	0.5 %	0.5 %	0.5 %
Total		100 %	100 %	100 %

Powder Flowability

Powder flowability was measured in triplicate using a ring shear tester (RST-XS; Dietmar Schulze, Wolfenbüttel, Germany), with a 10 mL cell at a 1 kPa pre-shear normal stress. A yield locus was obtained by plotting maximum shear stress as a function of normal stress (0.25, 0.40, 0.55, 0.70, and 0.85 kPa), from which unconfined yield strength (f_c) and major principal stress (σ_n) were obtained by drawing Mohr's circles. The flowability index was calculated as $ff_c = \frac{\sigma_n}{f_c}$.[39, 40]

Powder Compaction

A universal material test machine (Model 1485, Zwick/Roell, Germany) was used to prepare tablets at compaction pressures ranging from 25–350 MPa at a tableting speed of 4 mm/min. The punch tip and die wall were lubricated using a 5% (*w*/*v*) suspension of MgSt in ethanol, which was air-dried with a fan for ~1 min to complete dryness. Tablets were relaxed under ambient environment for at least 24 h before being diametrically broken using a texture analyzer (TA-XT2i; Texture Technologies Corporation, Scarsdale, NY). Tablet tensile strength was calculated from the breaking force and tablet dimensions following the standard procedure.[41]

Expedited Friability

Tablet friability was determined by an expedited method to quantify the ability of compressed tablets to resist wearing and abrasion.[42] Coded tablets prepared under different pressures were weighed, individually coded, and loaded into a friabilator (Model F2, Pharma Alliance Group Inc., Santa Clarita, CA), which rotated at 25 rpm for 4 min. The initial and final weight of each tablet was used to calculate percent weight loss, which was plotted against compaction pressure. The compaction pressure corresponding to 0.8% tablet weight loss was identified from the friability plot.

Dissolution performance

Tablet dissolution performance was determined in 250 mL pH 2.0 HCl (*aq*) at 37 ± 0.5 °C, which was paddle stirred at 50 rpm. Tablets were prepared at 200 MPa, each containing ~50 mg of IMC. Aliquots of the medium (3 mL) were taken at predetermined time points of 1, 3, 5, 10, 20, 30, 40, 50 and 60 min and passed through a filter membrane with a pore size of 0.45 μm. The IMC concentration was determined using a UV/Vis spectrophotometer (DU 500, Beckman Instruments, Fullerton, CA) at λ = 327 nm to avoid the interference from SAC using a calibration curve with appropriate background correction.

Solution ^{1}H Nuclear Magnetic Resonance (NMR) Spectroscopy

^{1}H NMR spectra were acquired on a Bruker Advance III HD 400 MHz spectrometer in DMSO-d_6 and referenced to the residual solvent resonance at δ 2.50 ppm. The pulse repetition delay was set at 10 s in the acquisition spectra for HPMC-containing samples. Anhydrous DMSO-d_6 solvent was distilled from activated molecular sieves and stored in an argon filled

glovebox with [H_2O] < 1 ppm. All NMR samples were prepared and sealed in the glovebox to avoid water uptake during the characterization.

Statistical Analysis

To assess statistical significance, the two-way analysis of variance (ANOVA) was performed. Difference between two data sets was deemed significant when $p < 0.05$.

Results and discussion

Micromeritic properties

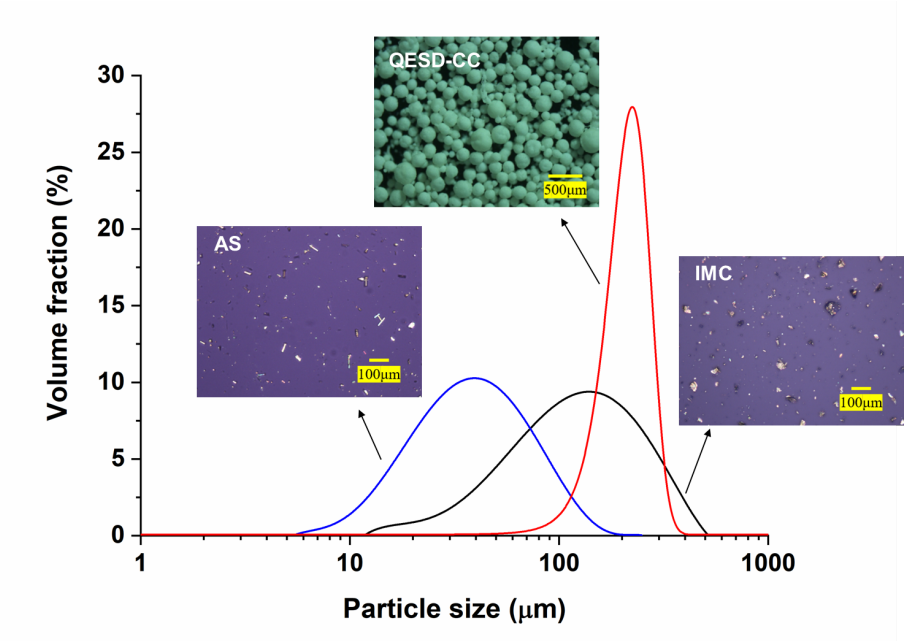

Figure 2. Particle size distributions of as-received IMC, and AS and QESD-CC powders, indicating that the QESD-CC yields highly spherical particles with a relatively narrower size distribution.

For the IMC-SAC system, phase purity of the obtained cocrystal was affected by both the [DMF]:[H_2O] solvent ratio and relative amounts of IMC and SAC. In preliminary studies, we

established that pouring a solution of 4 mmol IMC and 5 mmol SAC in 6 mL DMF into 40 mL of distilled water generated a phase pure IMC-SAC cocrystal. The use of HPMC during spherical crystallization significantly affected particle morphology, whereby a higher HPMC concentration led to larger size aggregates with more spherical shapes (Figure S1). However, high HPMC concentrations ($\geq$ 1 wt% in H_2O) led to process difficulties stemming from high solution viscosities that impede effective component mixing. Therefore, 0.5% (*w*/*v*) HPMC in the crystallization medium was used in the following studies. The resulting QESD-CC particles were highly spherical with a narrower particle size distribution than both as-received IMC and AS (Figure 2). In contrast, irregular IMC-SAC crystals were obtained when no HPMC was present in the crystallization medium (Figure S2). The effect of added HPMC is ascribed to its ability to stabilize the emulsions formed on mixing the drug solution with water. In the absence of HPMC, the emulsions were unstable and easily broke down under agitation, resulting in the production of fine individual crystals. Similar observations have been reported with celecoxib,[26] ketoprofen,[43] and bucillamine.[24]

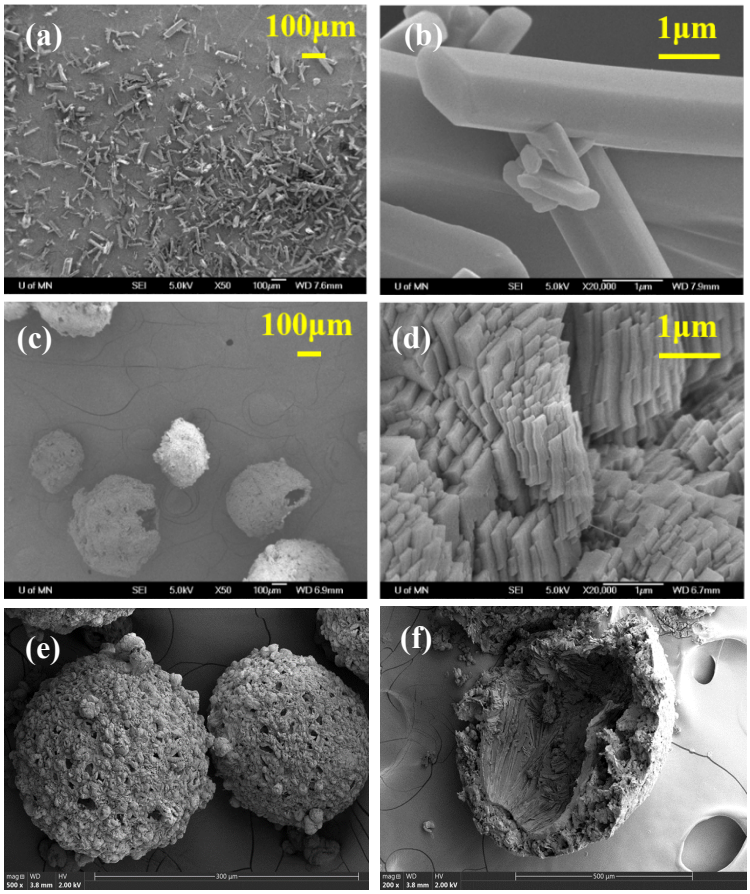

Figure 3. SEM images of particles prepared by the AS (a and b) and QESD-CC (c and d) processes at low (x 50) and high (x 20,000) magnifications. Images e) and f) demonstrate the hollow structure of QESD-CC particles

The SEM images revealed that primary IMC-SAC crystals prepared by the anti-solvent process (AS) consisted of both small and large micro-size crystals (Figures 3a, b). This is consistent with the broad PSD observed by laser scattering (Figure 2). Although large spherical agglomerates were present in the QESD-CC powder (Figure 2c), primary crystals in AS powder were much larger than those obtained by QESD-CC (Figure 3d). The broad PSD of AS powder was attributed to the preparation method, where a methanol solution of IMC and SAC was rapidly added (in ≤ 10 s) to an equal volume of water. In this process, the MeOH:H_2O volume

ratio is initially high, leading to a high degree of supersaturation of the IMC-SAC and instant precipitation of small micro-size IMC-SAC cocrystals. With continuous addition of methanol, the degree of supersaturation is lower than that at the beginning of the process because the more methanol-rich solvent can dissolve more IMC and SAC. Consequently, precipitation occurs more slowly, and the resulting crystals grow to larger sizes. However, during the QESD-CC process, the primary crystals were small (~ 1 μm) because the fast counter-diffusion between DMF and water (6:40, *v*/*v*) led to a high degree of supersaturation of IMC-SAC inside the emulsion droplets. Hence, fast nucleation limits the growth of individual primary crystals. The smaller size of primary IMC-SAC crystals in the QESD-CC powder corresponds well with the specific surface area (1.06 ±0.02 m^2/g) that was approximately twice that of IMC-SAC via anti-solvent (0.59 ±0.09 m^2/g). The spherical IMC-SAC particles obtained by QESD-CC appeared hollow with openings visible at the surface (Figure 3c, e). This hollow structure was confirmed by cutting a spherical cocrystal agglomerate to reveal the interior (Figure 3f).

Phase purity

The PXRD patterns of both AS and QESD-CC powders matched well with that calculated for IMC-SAC (Figure S3). This, along with the absence of characteristic peaks of individual crystals of IMC and SAC (Figure S3), indicates the formation of phase pure IMC-SAC cocrystals. The DSC thermograms of AS and QESD-CC powders (Figure S4) also corresponded well with the reported profiles of IMC-SAC.[30] The TGA profiles showed negligible weight loss on increasing the temperature to 153 °C (the boiling point of DMF), indicating the absence of any residual solvent in IMC-SAC prepared by both methods (Figure S5). The amount of HPMC in the QESD-CC powder prepared from a 0.5% HPMC solution was quantified as 0.67 ± 0.01 wt%, based on triplicate measurements.

Flowability and tabletability of various IMC forms

Both adequate flowability and tabletability of APIs are required for successfully manufacturing a high drug loading tablet by the DC process. The flow property of a powder is determined by gravity and adhesion, where gravity favors powder flow while adhesion hinders it.[44, 45] In general, larger and more spherical particles with smoother surfaces exhibit better flowability.[46] Given the larger size and more spherical shape of the QESD-CC particles as compared to those of AS and as-received IMC powders (Figure 2), the flowability of QESD-CC powder was significantly better than other forms of IMC in this study, as shown by the significantly higher ff_c ($p < 0.05$) (Figure 4a). Importantly, the flowability of the QESD-CC powder was significantly better than the Avicel PH102, which marks the minimum acceptable powder flowability for high speed tableting.[37] Hence, the flowability of the QESD-CC powder does not require further improvement by incorporating an excipient to sustain tablet ing.

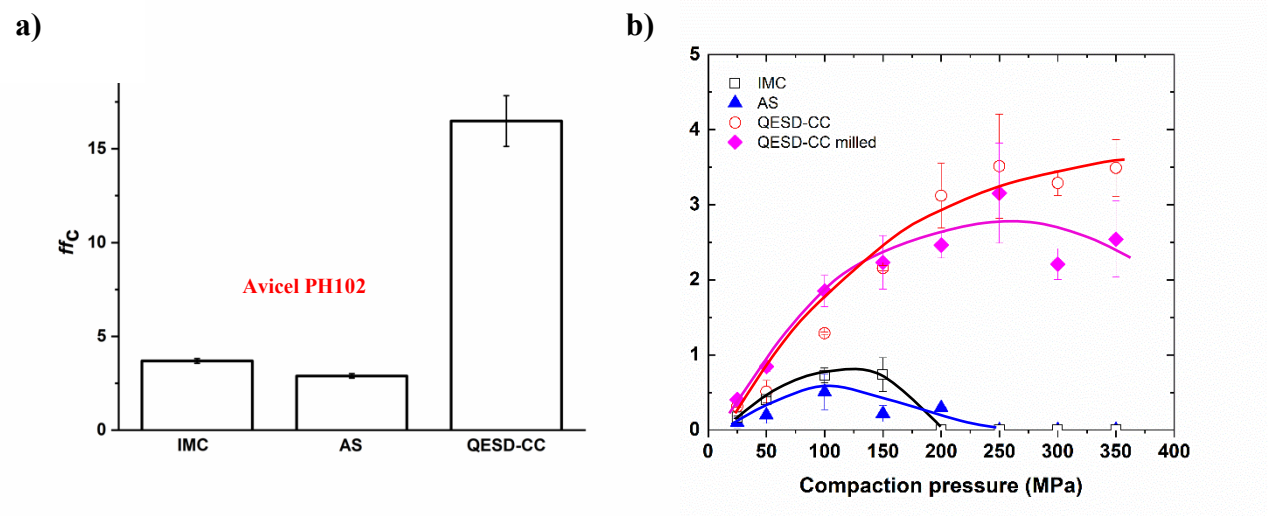

Figure 4. Powder properties of as-received IMC, AS, and QESD-CC powders, a) flowability and b) tabletability.

Both as-received IMC and AS powders showed poor tableting behavior (Figure 4b), which indicates inadequate plastic deformation that is required to develop sufficiently large bonding areas between particles in the tablet.[47] Therefore, crystal plasticity was assessed using a combined energy framework and topological analysis to gain structural insights.[48] In the γ-IMC crystal, the visually identified slip layers parallel to the (011) plane are energetically disfavored to slip due to strong interlayer interactions. On the other hand, the energetically more favorable molecular planes parallel to the (001) plane, recognized by an energy framework analysis, can undergo only very restricted slip because of the rough layer surface topology (Figure 5a).[32] In the IMC-SAC cocrystals, SAC-SAC and IMC-IMC dimers are held together through N-H···O (2.859 Å) and O-H···O (2.659 Å) hydrogen bonds, respectively. Those dimers assemble in 2D layers extending along the (001) plane through O-H···O=C (3.005 Å) and O-H···O=S (2.964 Å) hydrogen bonds. Only weak interactions between the neighboring layers, mediated by the edge to face π-π interactions (3.490 Å) and C-H···Cl (3.539 Å) hydrogen bonds were observed. This is consistent with the energy framework, which suggests (001) as the most likely primary slip plane in IMC-SAC (Figure 5b). However, such molecular layers are interlocked, due to the rough topology of the layer surface, as shown by the negative interlayer distance (-0.2 Å). The structural analyses above suggest that the poor plasticity of both IMC and IMC-SAC can be attributed to the absence of active slip systems.

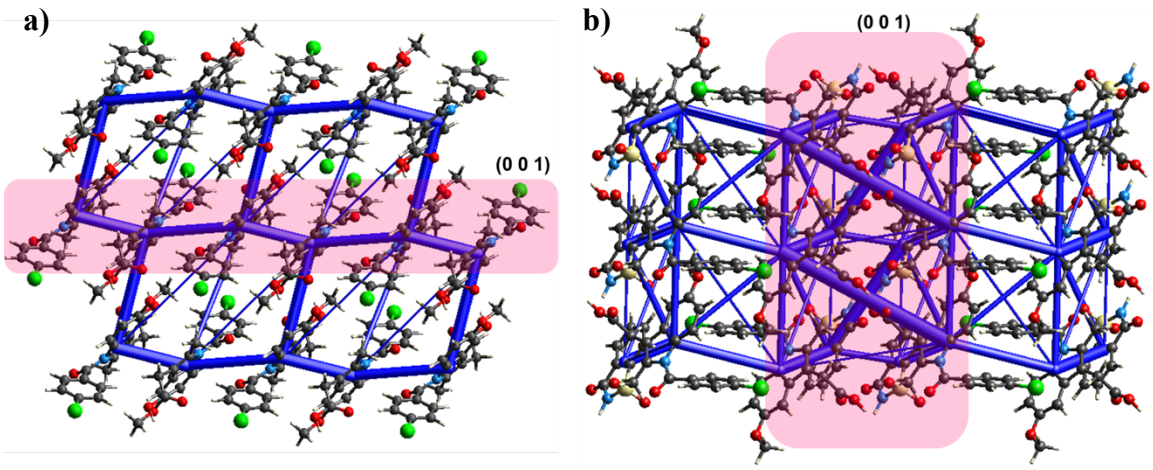

Figure 5. Energy frameworks for (a) IMC and (b) IMC-SAC with a likely slip plane shaded in pink. The thickness of each cylinder (*blue*) represents the relative strength of intermolecular interaction. The energy threshold for the energy framework is set at −10 kJ/mol.

However, the QESD-CC powder exhibited profoundly improved tableting performance relative to AS ($p < 0.05$), even though they are the same crystal polymorph. The highest tensile strength of ~ 3.6 MPa was approximately 6 times that of AS (~ 0.6 MPa) (Figure 4b). At 150 MPa compaction pressure, the tablet tensile strength was already higher than 2 MPa, suggesting adequate tablet mechanical strength for handling and processing under a relatively mild compaction pressure.[49] At least two factors can contribute to the improved tabletability: 1) coating of the crystals by HPMC and 2) much smaller primary crystal size. Surface coating is an effective particle engineering strategy to improve tabletability by increasing bonding area. Therefore, incorporation of as little as 0.67 wt% HPMC significantly improves tabletability.[19, 50, 51] Smaller primary crystal size furnishes a larger surface area available for bonding, thus favoring stronger tablets.[52] We excluded the fracture of large QESD-CC particles as a major factor, because the tabletability of the QESD-CC powder after milling for 5 min remained nearly identical below 250 MPa (Figure 4b).

Formulation development

The excellent flow and tableting properties of QESD-CC are expected to enable the formulation development of DC tablet with a high IMC loading. The blend of components in a successful DC tablet formulation must be sufficiently free flowing to make tablets with consistent weight and uniform drug content during high-speed tablet manufacturing. In this regard, the QESD-CC formulation meets the minimum flowability criterion, since it exhibits better flowability than Avicel PH102, while IMC and AS formulations do not (Figure 6a). This result highlights the important role of the API on the flowability of high drug loading formulations.

The tableting performance of formulations followed the same order as that of API powders, i.e., QESD-CC > as received IMC > AS. When the compaction pressure was higher than 200 MPa, the tablet tensile strength for all formulations exceeded 2 MPa (Figure 6b), despite both as-received IMC and AS powders exhibiting poor tabletability with maximum tensile strengths of approximately 0.6 and 0.5 MPa, respectively (Figure 4b). The improved tabletability indicates that the presence of plastic Avicel PH102 (24.5 wt% in cocrystal formulations and 48.2 wt% in IMC formulation) could overcome the poor tabletability of API in both formulations. This is attributed to the excellent tabletability of Avicel PH102.[53] Considering the otherwise identical composition between QESD-CC and AS formulations (Table 1), the better tabletability of QESD-CC formulation than AS formulation suggests that the tableting performance of API also influences tabletability of high dose DC tablet formulations (Figure 4b).

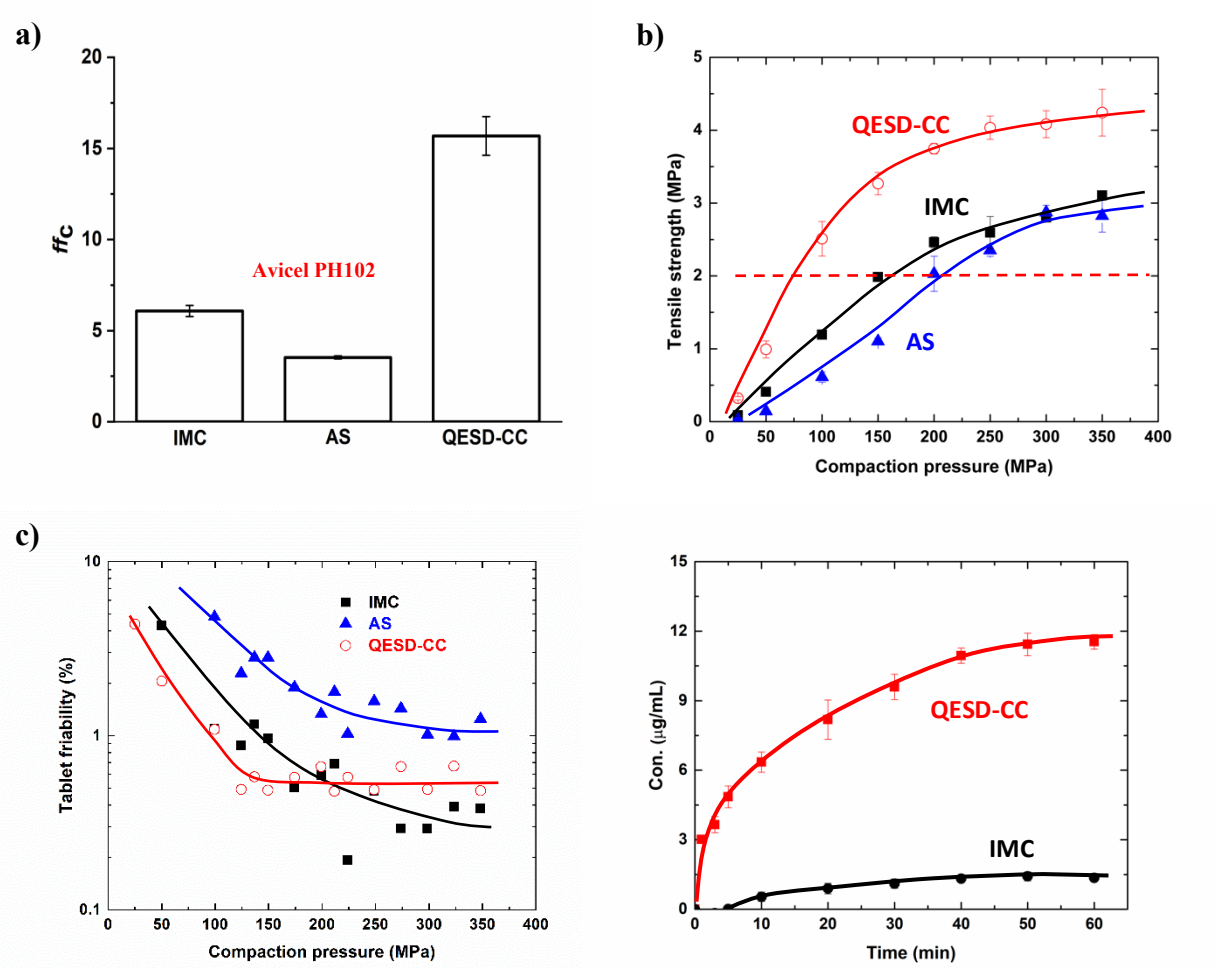

Figure 6. Performance of tablet formulations based on as-received IMC, AS, and QESD-CC, (a) flowability, (b) tabletability, c) tablet friability, and d) tablet dissolution.

Friability characterizes the propensity of a tablet to lose mass when exposed to external impact during downstream processing, shipping, and handling.[54] The friability of IMC and QESD-CC formulations met the friability requirement that tablets compressed at compaction pressures higher than 150 MPa and 100 MPa, respectively, exhibited weight loss of ≤ 0.8%. The tablet friability of AS formulation remained higher than 0.8% in the entire range of compaction pressure (Figure 6c). Therefore, it is unlikely to be a successful DC tablet formulation.

Dissolution

The final remaining consideration for assessing the suitability of the DC process is dissolution. Tablets containing 50 mg of as-received IMC or an equivalent amount of QESD-CC (75.6 mg) were prepared at a compaction pressure of 200 MPa, and their dissolution performance was determined in simulated gastric fluid (250 mL of pH 2.0 HCl aqueous solution). The 200 MPa compaction pressure was used because tablets from both formulations exhibited sufficient mechanical strength, as shown by > 2 MPa tensile strength (Figure 6b) and < 0.8% friability (Figure 6c). As expected, the formulated QESD-CC showed much improved drug release compared to IMC, with the area under curve of QESD-CC being ~9-fold higher than IMC (Figure 6d). Thus, the dissolution data confirms that the QESD-CC approach can indeed be used to enable the development of high dose DC tablets of IMC.

Drug-polymer molecular interaction

To better understand the mechanism in formation of the spherical cocrystal agglomerates, we further probed the underlying intermolecular interactions between HPMC and IMC/SAC molecules by solution ^{1}H NMR. To mimic the aqueous environment in the QESD process, deuterium oxide would be the ideal solvent to use. However, the poor water solubility of IMC led us to characterize these interactions in DMSO-d_6 in order to co-dissolve all three components involved in this process.

When the concentration of IMC-SAC in DMSO-d_6 increased from 2 to 8 mg/mL, the peaks positions correlated with IMC at δ 7.60–7.70 ppm did not change (Figure 7a). However, downfield shifts of ^{1}H NMR spectral peaks were observed in the range δ 7.80–8.20 ppm (Figure 7a), which correspond to the H atom resonances on the aromatic ring of SAC (Figures 1b). The downfield shift indicates decreased electron density in the aromatic ring, which is induced by a

stronger hydrogen bonding between adjacent SAC molecules through amide moieties, which is analogous to the amide dimer (N-H···O; 2.859(3) Å) synthon (R^2_2 (8) motif) formed between two SAC molecules in the IMC-SAC crystal structure as depicted in Figure 7c. With the addition of 0.5 mg/mL HPMC to a 2 mg/mL IMC-SAC solution, an upfield shift of these peaks is observed that suggests weakening of the N-H···O H-bond between SAC dimers induced by HPMC through competitive hydrogen bonding interactions (Figure 7a). Additionally, the peaks corresponding to the -OH substituents on HPMC broaden in the presence of IMC-SAC (Figure 7b), corroborating their conformational restrictions imposed by participation in hydrogen bonding interactions with the SAC molecules. Similar peak shifts and peak smearing in ^{1}H NMR spectra of SAC and HPMC were observed in the absence of IMC (Figure S6). These observations suggest that the hydroxyl groups on HPMC form hydrogen bonds with SAC, which weaken the originally strong intermolecular N-H···O hydrogen bonds between SAC molecules while IMC is not directly involved. Since the ^{1}H NMR spectra of IMC remained the same in the presence and absence of HPMC (Figure 7a), IMC does not significantly interact with HPMC.

The preferential interaction of HPMC with SAC instead of IMC was further investigated using DFT computational simulations, which revealed hydrogen bonds formed between SAC and HPMC monomer units through S=O···H-O (2.889 Å), N-H···O (2.704 Å, 2.832 Å), and C=O···H-O (2.775 Å) interactions (Figure 8). In comparison, no hydrogen bonds between HPMC and IMC were suggested by the simulations. These results corroborate the intermolecular interactions inferred from the ^{1}H NMR data (Figures 7 and S6), i.e., the dominant intermolecular interactions between HPMC and IMC-SAC are hydrogen bonds between SAC and HPMC.

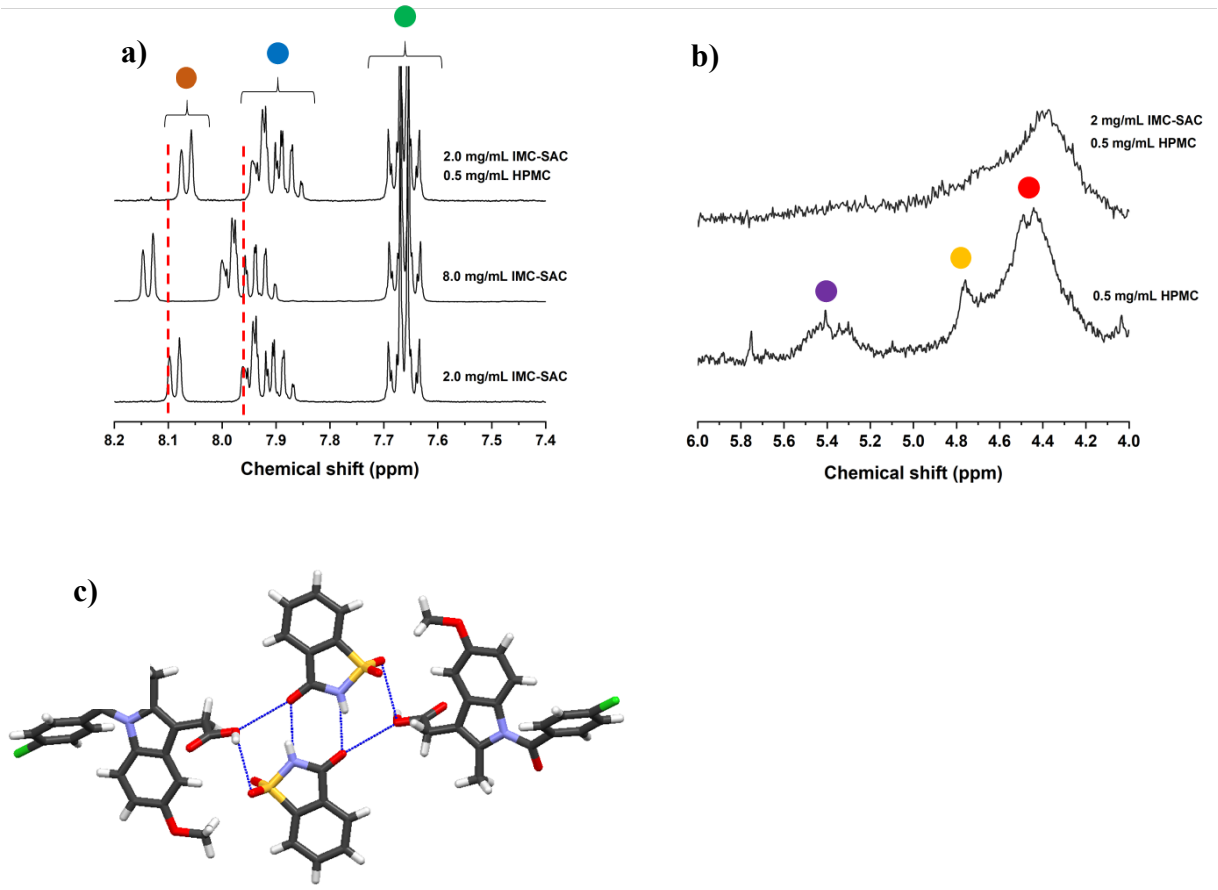

Figure 7. Partial ^{1}H NMR spectra of (a) 2 mg/mL IMC-SAC (bottom), 2 mg/mL IMC-SAC with 0.5 mg/mL HPMC (top) and 8 mg/mL IMC-SAC (middle), and (b) 0.5 mg/mL HPMC with and without 2 mg/mL of IMC-SAC (colored dots correspond to the H atoms labeled in Figure 1), (c) Intermolecular hydrogen bonding interactions (blue lines) in IMC-SAC.

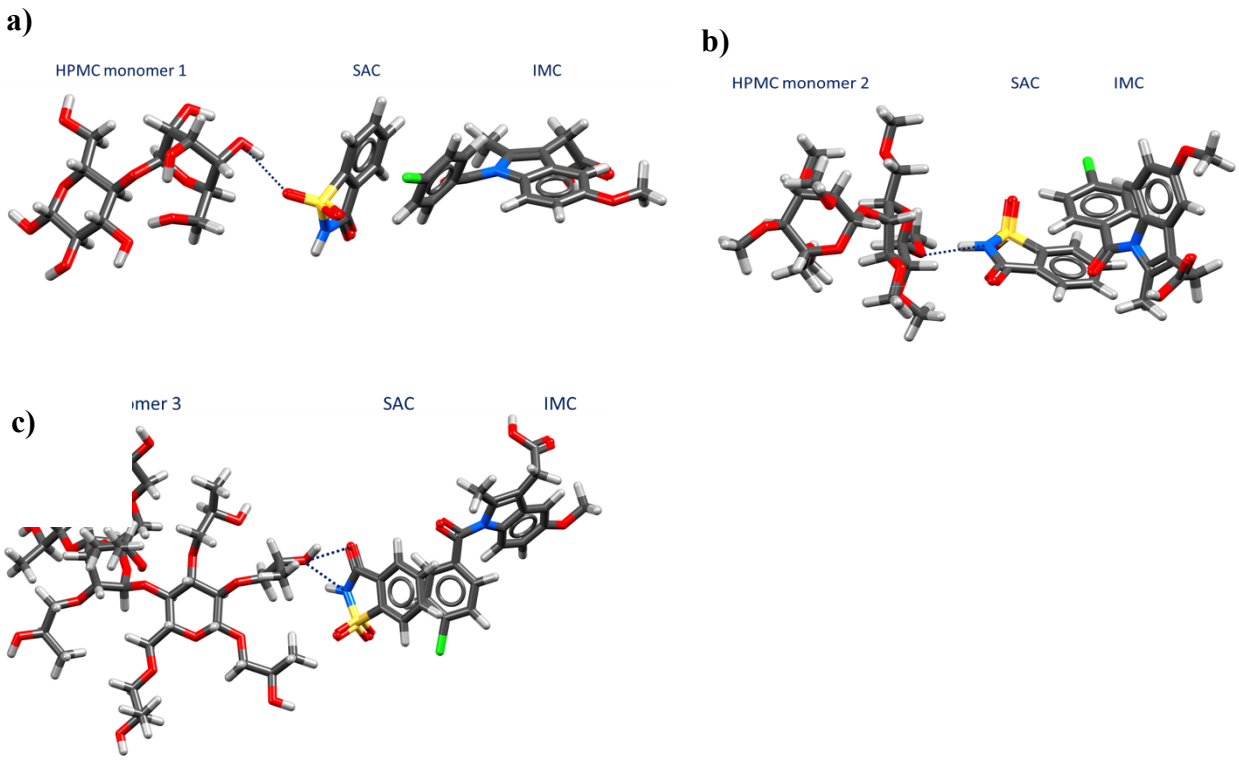

Figure 8. Optimized geometric complexes between IMC-SAC and three HPMC monomer units with different substituents: a) -H, b) $-CH_3$, c) $-CH_2CH(OH)CH_3$.

Formation mechanism of spherical cocrystal agglomerates

The observed hollow structure of the QESD-CC particles (Figures 3e,f) provides some insights into a possible formation mechanism. Emulsion droplets first form on mixing the concentrated drug solution and aqueous medium. HPMC in the aqueous medium interacts with SAC at the organic-aqueous interface through the hydrogen bonds described above to stabilize the emulsion (Figure 9c). The counter diffusion of water and DMF drives a high degree of supersaturation near the drop surface and results in the precipitation of very fine IMC-SAC crystals to form a crust. As DMF diffuses into the aqueous phase, interfacially-adsorbed HPMC precipitates and coats the surface of the particles because of the poorer solubility of HPMC in the

DMF-rich solvent mixture adjacent to the particle surface. The crust grows inward as the solvent counter diffusion continues until cocrystallization is complete. This process naturally leads to particles with a core-shell structure with a HPMC coating. Upon drying, the entrapped solvent escapes through pores in the shell by evaporation. This particle formation mechanism is consistent with the greatly enhanced tabletability, which is possible if HPMC coats the QESD-CC particles instead of distributing throughout the bulk. Additionally, such hollow particles are more deformable during compression, which maximizes the interparticle contact area and favors higher tablet strength.

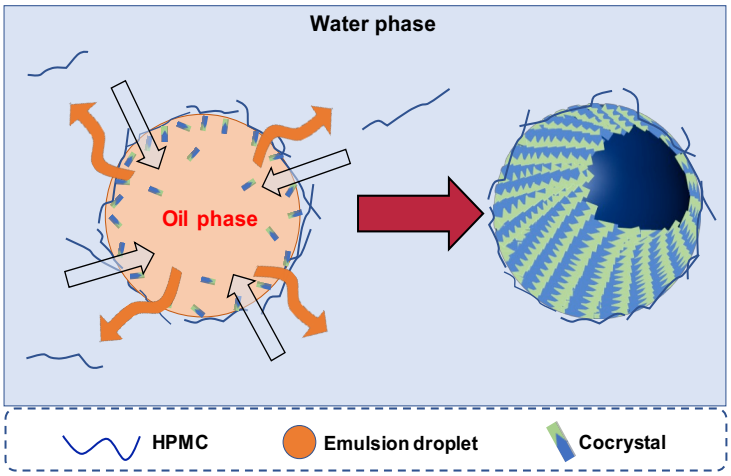

Figure 9. An illustration of the process of forming a QESD-CC particle.

Conclusion

We have designed and successfully applied a novel quasi-emulsion solvent diffusion cocrystallization (QESD-CC) method to simultaneously overcome poor flowability, poor tabletability, and slow dissolution of IMC. HPMC stabilizes the emulsion through hydrogen bond interactions with SAC molecules at the emulsion surface. Subsequent solvent counter-

diffusion leads to the initiation of the IMC-SAC crystallization at the emulsion drop surface. The cocrystal grows inward to form a core-shell structure, resulting in round and large sized QESD-CC particles, which exhibits excellent powder flowability. The HPMC coating of particle surface and much smaller size of primary IMC-SAC crystals account for significantly improved tabletability. The improved flowability and tabletability enable the successful manufacturing of a high IMC loading (46.3 wt%) tablet formulation using the direct compression process. Tablets also exhibited excellent dissolution due to the much higher solubility of the IMC-SAC cocrystal than IMC. Thus, for poorly soluble drugs that also exhibit poor flowability, the QESD-CC approach is a potentially highly effective and efficient engineering strategy to enable the successful manufacturing of high drug loading tablets using the most economical direct compression process.

ASSOCIATED CONTENT

Supporting Information. Optical microscopy micrographs of particles, calculated and experimental PXRD patterns, DSC and TGA thermograms, Partial ^{1}H NMR spectra of different solutions, SEC calibration curve, N2 physisorption isotherms, and intermolecular interaction energies. This material is available free of charge via the Internet at http://pubs.acs.org."

Acknowledgements

H.C. was partially supported by the Chinese Scholarship Council and David Grant and Marilyn Grant Fellowship in Physical Pharmacy (2019-2020), Department of Pharmaceutics, University of Minnesota. H. X. and M. K. M. gratefully acknowledge National Science

Foundation DMR-1708874. Contributions from H.K. and C.L.H. were supported by the National Science Foundation under the Center for Sustainable Nanotechnology, CHE-1503408; the CSN is part of the Centers for Chemical Innovation Program. SEM analyses were performed in the College of Science and Engineering Characterization Facility at the University of Minnesota, which receives partial support from National Science Foundation through the UMN MRSEC (DMR-1420013). Portions of this work were conducted in the Minnesota Nano Center, which is supported by the National Science Foundation through the National Nano Coordinated Infrastructure Network (NNCI) under Award Number ECCS-1542202. We thank the Minnesota Supercomputing Institute (MSI) at the University of Minnesota for providing resources that contributed to the research results reported in this paper. URL: http://www.msi.umn.edu.

References

1. Van Snick, B.; Holman, J.; Cunningham, C.; Kumar, A.; Vercruysse, J.; De Beer, T.; Remon, J. P.; Vervaet, C. Continuous direct compression as manufacturing platform for sustained release tablets. *Int J. Pharm.* **2017**, 519, 390-407.
2. Jivraj, M.; Martini, L. G.; Thomson, C. M. An overview of the different excipients useful for the direct compression of tablets. *Pharm. Sci. Technol. Today* **2000**, 3, 58-63.
3. Chen, H.; Aburub, A.; Sun, C. C. Direct compression tablet containing 99% active ingredient—a tale of spherical crystallization. *J. Pharm. Sci.* **2019**, 108, 1396-1400.
4. Chen, L.; Ding, X.; He, Z.; Huang, Z.; Kunnath, K. T.; Zheng, K.; Davé, R. N. Surface engineered excipients: I. Improved functional properties of fine grade microcrystalline cellulose. *Int. J. Pharm.* **2018**, 536, 127-137.
5. Kawashima, Y.; Okumura, O.; Takenaka, H. Spherical crystallization direct spherical agglomeration of salicylic acid crystals during crystallization. *Science* **1982**, 216, 1127-1128.
6. Chen, H.; Wang, C.; Sun, C. C. Profoundly improved plasticity and tabletability of griseofulvin by in situ solvation and desolvation during spherical crystallization. *Cryst. Growth Des.* **2019**, 19, 2350-2357.
7. Peña, R.; Nagy, Z. K. Process intensification through continuous spherical crystallization using a two-stage mixed suspension mixed product removal (msmpr) system. *Cryst. Growth Des.* **2015**, 15, 4225-4236.
8. Kawashima, Y.; Niwa, T. Preparation of controlled-release microspheres of ibuprofen with acrylic polymers by a novel quasi-emulsion solvent diffusion method. *J. Pharm. Sci.* **1988**, 78, 68-72.
9. Tahara, K.; O'Mahony, M.; Myerson, A. S. Continuous spherical crystallization of albuterol sulfate with solvent recycle system. *Cryst. Growth Des.* **2015**, 15, 5149-5156.
10. Chen, H.; Wang, C.; Kang, H.; Zhi, B.; Haynes, C. L.; Aburub, A.; Sun, C. C. Microstructures and pharmaceutical properties of ferulic acid agglomerates prepared by different spherical crystallization methods. *Int. J. Pharm.* **2020**, 574, 118914.

11. Saboo, S.; Mugheirbi, N. A.; Zemlyanov, D. Y.; Kestur, U. S.; Taylor, L. S. Congruent release of drug and polymer: A "sweet spot" in the dissolution of amorphous solid dispersions. *J. Control. Release* **2019**, 298, 68-82.
12. Serajuddin, A. T. Salt formation to improve drug solubility. *Adv. Drug Deliv. Rev.* **2007**, 59, 603-616.
13. Blagden, N.; de Matas, M.; Gavan, P. T.; York, P. Crystal engineering of active pharmaceutical ingredients to improve solubility and dissolution rates. *Adv. Drug Deliv. Rev* **2007**, 59, 617-630.
14. Han, R.; Xiong, H.; Ye, Z.; Yang, Y.; Huang, T.; Jing, Q.; Lu, J.; Pan, H.; Ren, F.; Ouyang, D. Predicting physical stability of solid dispersions by machine learning techniques. *J. Control. Release* **2019**, 311-312, 16-25.
15. Indulkar, A. S.; Lou, X.; Zhang, G. G. Z.; Taylor, L. S. Insights into the dissolution mechanism of ritonavir–copovidone amorphous solid dispersions: Importance of congruent release for enhanced performance. *Mol. Pharm.* **2019**, 16, 1327-1339.
16. Zheng, K.; Lin, Z.; Capece, M.; Kunnath, K.; Chen, L.; Davé, R. N. Effect of particle size and polymer loading on dissolution behavior of amorphous griseofulvin powder. *J. Pharm. Sci.* **2019**, 108, 234-242.
17. Aitipamula, S.; Banerjee, R.; Bansal, A. K.; Biradha, K.; Cheney, M. L.; Choudhury, A. R.; Desiraju, G. R.; Dikundwar, A. G.; Dubey, R.; Duggirala, N.; Ghogale, P. P.; Ghosh, S.; Goswami, P. K.; Goud, N. R.; Jetti, R. R. K. R.; Karpinski, P.; Kaushik, P.; Kumar, D.; Kumar, V.; Moulton, B.; Mukherjee, A.; Mukherjee, G.; Myerson, A. S.; Puri, V.; Ramanan, A.; Rajamannar, T.; Reddy, C. M.; Rodriguez-Hornedo, N.; Rogers, R. D.; Row, T. N. G.; Sanphui, P.; Shan, N.; Shete, G.; Singh, A.; Sun, C. C.; Swift, J. A.; Thaimattam, R.; Thakur, T. S.; Kumar Thaper, R.; Thomas, S. P.; Tothadi, S.; Vangala, V. R.; Variankaval, N.; Vishweshwar, P.; Weyna, D. R.; Zaworotko, M. J. Polymorphs, salts, and cocrystals: What's in a name? *Crys. Growth Des.* **2012**, 12, 2147-2152.
18. Drozd, K. V.; Manin, A. N.; Churakov, A. V.; Perlovich, G. L. Novel drug–drug cocrystals of carbamazepine with para-aminosalicylic acid: Screening, crystal structures and comparative study of carbamazepine cocrystal formation thermodynamics. *CrystEngComm* **2017**, 19, 4273-4286.
19. Chen, H.; Guo, Y.; Wang, C.; Dun, J.; Sun, C. C. Spherical cocrystallization—an enabling technology for the development of high dose direct compression tablets of poorly soluble drugs. *Cryst. Growth Des.* **2019**, 19, 2503-2510.
20. Pagire, S. K.; Korde, S. A.; Whiteside, B. R.; Kendrick, J.; Paradkar, A. Spherical crystallization of carbamazepine/saccharin co-crystals: Selective agglomeration and purification through surface interactions. *Crys. Growth Des.* **2013**, 13, 4162-4167.
21. Sun, C. C. Decoding powder tabletability: Roles of particle adhesion and plasticity. *J. Adhes. Sci. Technol.* **2011**, 25, 483-499.
22. Kakran, M.; Sahoo, N. G.; Tan, I.-L.; Li, L. Preparation of nanoparticles of poorly water-soluble antioxidant curcumin by antisolvent precipitation methods. *J. Nanopart. Res.* **2012**, 14, 757.
23. Chun, N.-H.; Wang, I.-C.; Lee, M.-J.; Jung, Y.-T.; Lee, S.; Kim, W.-S.; Choi, G. J. Characteristics of indomethacin–saccharin (imc–sac) co-crystals prepared by an anti-solvent crystallization process. *Eur. J. Pharm. Biopharm.* **2013**, 85, 854-861.
24. Morishima, K.; Kawashima, Y.; Kawashima, Y.; Takeuchi, H.; Niwa, T.; Hino, T. Micromeritic characteristics and agglomeration mechanisms in the spherical crystallization of bucillamine by the spherical agglomeration and the emulsion solvent diffusion methods. *Powder Technol.* **1993**, 76, 57-64.
25. Kenji, M.; Yoshiaki, K.; Hirofumi, T.; Toshiyuki, N.; Tomoaki, H.; Yoichi, K. Tabletting properties of bucillamine agglomerates prepared by the spherical crystallization technique. *Int. J. Pharm.* **1994**, 105, 11-18.

26. Chen, H.; Paul, S.; Xu, H.; Wang, K.; Mahanthappa, M. K.; Sun, C. C. Reduction of punch-sticking propensity of celecoxib by spherical crystallization via polymer assisted quasi-emulsion solvent diffusion. *Mol. Pharm.* **2020**, 17, 1387–1396.
27. Alhalaweh, A.; Roy, L.; Rodríguez-Hornedo, N.; Velaga, S. P. Ph-dependent solubility of indomethacin–saccharin and carbamazepine–saccharin cocrystals in aqueous media. *Mol. Pharm.* **2012**, 9, 2605-2612.
28. Brunauer, S.; Emmett, P. H.; Teller, E. Adsorption of gases in multimolecular layers. *J. Am. Chem. Soc.* **1938**, 60, 309-319.
29. Chen, M.-H.; Bergman, C. J. Method for determining the amylose content, molecular weights, and weight- and molar-based distributions of degree of polymerization of amylose and fine-structure of amylopectin. *Carbohydr. Polym.* **2007**, 69, 562-578.
30. Basavoju, S.; Boström, D.; Velaga, S. P. Indomethacin–saccharin cocrystal: Design, synthesis and preliminary pharmaceutical characterization. *Pharm. Res.* **2008**, 25, 530-541.
31. Turner, M. J.; Thomas, S. P.; Shi, M. W.; Jayatilaka, D.; Spackman, M. A. Energy frameworks: Insights into interaction anisotropy and the mechanical properties of molecular crystals. *Chem. Comm.* **2015**, 51, 3735-3738.
32. Wang, C.; Sun, C. C. Identifying slip planes in organic polymorphs by combined energy framework calculations and topology analysis. *Cryst. Growth Des.* **2018**, 18, 1909-1916.
33. Turner, M. J.; Grabowsky, S.; Jayatilaka, D.; Spackman, M. A. Accurate and efficient model energies for exploring intermolecular interactions in molecular crystals. *J. Phys. Chem. Lett.* **2014**, 5, 4249-4255.
34. Bryant, M. J.; Maloney, A. G. P.; Sykes, R. A. Predicting mechanical properties of crystalline materials through topological analysis. *CrystEngComm* **2018**, 20, 2698-2704.
35. Paul, S.; Sun, C. C. Dependence of friability on tablet mechanical properties and a predictive approach for binary mixtures. *Pharm. Res.* **2017**, 34, 2901-2909.
36. Zhao, Y.; Truhlar, D. G. J. T. C. A. The m06 suite of density functionals for main group thermochemistry, thermochemical kinetics, noncovalent interactions, excited states, and transition elements: Two new functionals and systematic testing of four m06-class functionals and 12 other functionals. *Theor. Chem. Acc.* **2008**, 120, 215-241.
37. Sun, C. C. Setting the bar for powder flow properties in successful high speed tableting. *Powder Technol.* **2010**, 201, 106-108.
38. Chen, L.; Ding, X.; He, Z.; Fan, S.; Kunnath, K. T.; Zheng, K.; Davé, R. N. Surface engineered excipients: Ii. Simultaneous milling and dry coating for preparation of fine-grade microcrystalline cellulose with enhanced properties. *Int. J. Pharm.* **2018**, 546, 125-136.
39. Shi, L.; Chattoraj, S.; Sun, C. C. Reproducibility of flow properties of microcrystalline cellulose — avicel ph102. *Powder Technol.* **2011**, 212, 253-257.
40. Schulze, D. Powders and bulk solids: Behavior, characterization, storage and flow, springer, berlin, heidelberg, new york, tokyo, 2008.
41. Fell, J. T.; Newton, J. M. Determination of tablet strength by the diametral-compression test. *J. Pharm. Sci.* **1970**, 59, 688-691.
42. Osei-Yeboah, F.; Sun, C. C. Validation and applications of an expedited tablet friability method. *Int. J. Pharm.* **2015**, 484, 146-155.
43. Ribardière, A.; Tchoreloff, P.; Couarraze, G.; Puisieux, F. Modification of ketoprofen bead structure produced by the spherical crystallization technique with a two-solvent system. *Int. J. Pharm.* **1996**, 144, 195-207.
44. Chattoraj, S.; Shi, L.; Sun, C. C. Profoundly improving flow properties of a cohesive cellulose powder by surface coating with nano-silica through comilling. *J. Pharm. Sci.* **2011**, 100, 4943-4952.
45. Kendall, K. Adhesion: Molecules and mechanics. *Science* **1994**, 263, 1720-1725.

46. Hou, H.; Sun, C. C. Quantifying effects of particulate properties on powder flow properties using a ring shear tester. *J. Pharm. Sci.* **2008**, 97, 4030-4039.
47. Sun, C. C.; Kleinebudde, P. Mini review: Mechanisms to the loss of tabletability by dry granulation. *Eur. J. Pharm. Biopharm.* **2016**, 106, 9-14.
48. Wang, C.; Sun, C. C. Computational techniques for predicting mechanical properties of organic crystals: A systematic evaluation. *Mol. Pharm.* **2019**, 16, 1732-1741.
49. Sun, C. C.; Hou, H.; Gao, P.; Ma, C.; Medina, C.; Alvarez, F. J.; Hou, H.; Gao, P. Development of a high drug load tablet formulation based on assessment of powder manufacturability: Moving towards quality by design. *J. Pharm. Sci.* **2009**, 98, 239-247.
50. Shi, L.; Sun, C. C. Overcoming poor tabletability of pharmaceutical crystals by surface modification. *Pharm. Res.* **2011**, 28, 3248-3255.
51. Shi, L.; Sun, C. C. Transforming powder mechanical properties by core/shell structure: Compressible sand. *J. Pharm. Sci.* **2010**, 99, 4458-4462.
52. Shi, L.; Feng, Y.; Sun, C. C. Roles of granule size in over-granulation during high shear wet granulation. *J. Pharm. Sci.* **2010**, 99, 3322-3325.
53. Zhang, Y.; Law, Y.; Chakrabarti, S. Physical properties and compact analysis of commonly used direct compression binders. *AAPS PharmSciTech.* **2003**, 4, 489-499.
54. Sinka, I. C.; Cunningham, J. C.; Zavaliangos, A. Analysis of tablet compaction. Ii. Finite element analysis of density distributions in convex tablets. *J. Pharm. Sci.* **2004**, 93, 2040-2053.

For Table of Contents Use Only

A Novel Quasi-Emulsion Solvent Diffusion based Spherical Cocrystallization Strategy for Simultaneously Improving the Manufacturability and Dissolution of Indomethacin

Hongbo Chen, Hongyun Xu, Chenguang Wang, Hyunho Kang, Christy L. Haynes, Mahesh K. Mahanthappa, and Changquan Calvin Sun*

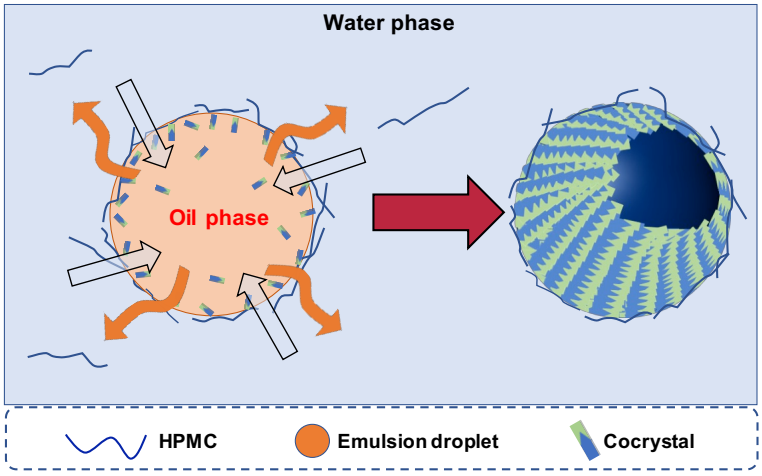

Synopsis:

Spherical indomethacin-saccharin cocrystal agglomerates were formed by a quasi-emulsion solvent diffusion (QESD) process with HPMC as an emulsion stabilizer. Hollow cocrystal agglomerates form by rapid cocrystal precipitation near the surface of the HPMC-stabilized emulsion droplets, due to the counter diffusion of water and organic solvent, followed by slow inward growth.